ELSEVIER

Comput. Methods Appl. Mech. Engrg. 113 (1994) 397–414

Computer methods in applied mechanics and engineering

A new implementation of the element free Galerkin method

Y.Y. Lu, T. Belytschko,*, L. Gu

Department of Civil Engineering, Robert R. McCormick School of Engineering and Applied Science, The Technological Institute, Northwestern University, Evanston, IL 60208-3019, USA

Received 11 June 1993

Abstract

Element free Galerkin methods (EFG) are methods for solving partial differential equations with moving least squares interpolants. EFG methods require only nodal data; no element connectivity is needed. In a previous implementation of the EFG method, Lagrange multipliers were used to enforce the essential boundary condition. However, the use of Lagrange multipliers increases the cost of solving the linear algebraic equations. A new implementation is developed based on a modified variational principle in which the Lagrange multipliers are replaced at the outset by their physical meaning so that the discrete equations are banded. In addition, weighted orthogonal basis functions are constructed so the need for solving equations at each quadrature point is eliminated. Numerical examples show that the present implementation effectively computes stress concentrations and stress intensity factors at cracks with very irregular arrangements of nodes; the latter makes it very advantageous for modelling progressive cracking.

1. Introduction

The element free Galerkin method (EFG), which is based on moving least square interpolants, is a promising method for treatment of problems such as progressive crack growth because it does not require any element connectivity data and does not suffer much degradation in accuracy when nodal arrangements are very irregular. Thus, in crack growth problems, nodes can be arranged around a crack to capture the stress intensity factors with the requisite accuracy and moved through another arrangement of nodes associated with the global geometry. In addition, meshing for a large variety of problems, including linear and nonlinear stress analyses by adaptive methods, can be effectively treated by this method in a simple manner.

At least two forms of this method have been reported. Nayroles et al. [1], who were the first to report this class of methods, used a very low order quadrature and did not enforce essential boundary conditions exactly. They called their method 'diffuse elements'; they did not recognize that they used moving least square (MLS) interpolants. Belytschko et al. [2] developed an alternate implementation which emphasizes accuracy. To achieve this accuracy they used:

(1) Lagrange multipliers to enforce the essential boundary conditions;
(2) high-order quadrature based on a background mesh of regular cells.

It was discovered by Belytschko et al. [2] in elasticity and heat conduction that their implementation of element free Galerkin method possesses the following noteworthy advantages:

(1) it does not exhibit any volumetric locking, even when the basis function is linear;
(2) the rate of convergence for the method can exceed that of finite elements significantly;
(3) a high resolution of localized steep gradients can be achieved.

* Corresponding author.

SSDI 0045-7825(93)E0119-S

In the element free Galerkin method, MLS interpolants are used for the trial and test functions with a variational principle (weak form); see for example [3, 4] for descriptions of MLS. To use MLS interpolants, it is only necessary to construct an array of nodes in the domain under consideration. The method is therefore completely element free but can be imbued with the generality of a finite element method. Thus, key advantages of the EFG method compared to the finite element method are:

(1) Only a mesh of nodes and a boundary description are needed to develop the discrete equations (the element mesh is unnecessary).
(2) The dependent variable and its gradient are continuous in the entire domain and post-processing to obtain a smooth gradient field is totally unnecessary.

One disadvantage of MLS interpolants is that a set of linear algebraic equations must be solved for every spatial point at which the values of the primary dependent variables are to be calculated (see [3]). Therefore, in the element free Galerkin method, an $m \times m$ matrix, say $\boldsymbol{A}$, must be inverted for every quadrature point when the discrete equations are assembled. Similarly, in post-processing, $\boldsymbol{A}$ must be inverted at each point when the strains and stresses are computed. The computational cost associated with this is quite burdensome. Moreover, in order to retain the high accuracy of MLS interpolants, the matrix $\boldsymbol{A}$ must be inverted accurately; our experience indicates that accuracy is compromised if the inverse of matrix $\boldsymbol{A}$ is obtained inaccurately.

Another disadvantage of the Belytschko et al. [2] implementation of EFG method is that Lagrange multipliers are used to enforce the essential boundary condition. The essential boundary conditions cannot be enforced as easily as in finite element methods because moving least square interpolants do not pass through the data; this is a consequence of the fact that MLS interpolants are not equal to unity at the nodes unless the weighting functions are singular. It was shown in [2] that the EFG method does not satisfy the elementary patch test if the Nayroles et al. [1] implementation, which does not satisfy essential boundary conditions, is used. Since the patch test is equivalent to consistency, an essential requirement for convergence, the exact satisfaction of essential boundary conditions is imperative. However, the enforcement of essential boundary conditions by Lagrange multipliers increases the number of unknowns and leads to an awkward equation structure; the matrix which has to be inverted possesses zeroes on its main diagonal and solvers with variable bandwidth which do not take advantage of positive definiteness need to be employed. It should be noted that the use of Lagrange multipliers is also extremely unwieldy for dynamic problems.

In order to ameliorate these two shortcomings, a new implementation of the EFG method is described in this paper. First, weighted orthogonal basis functions are constructed for the MLS interpolants by using a Schmidt orthogonalization. With the use of the weighted orthogonal basis functions, the burden of inverting the matrix $\boldsymbol{A}$ at quadrature points is totally eliminated.

To circumvent the use of Lagrange multipliers yet maintain the satisfaction of essential boundary conditions, we consider the physical meaning of the Lagrange multipliers. In many physical problems, the Lagrange multipliers can be identified with physical quantities (such as boundary tractions in elasticity and the boundary flux in heat conduction). Therefore, a modified variational principle can be established in which the Lagrange multipliers are replaced at the outset by its physical counterpart [5, 6]. Such modified variational principles tend not to work very well with finite element methods, particularly those of low order, because the implicit Lagrange multiplier is a lower order field than the variable which is constrained. However, with the MLS interpolants, the modified variational principle appears to perform quite well for reasonable numbers of unknowns. Since this modified variational principle results in a positive definite, banded matrix, it becomes quite appealing.

This paper is organized as follows. In Section 2, the development of weighted orthogonal basis functions for the MLS interpolant is described. In Section 3, the modified variational principle for obtaining the discrete equations for the EFG method is given, along with the implementation of the method. Numerical results are presented in Section 4 in order to assess the effectiveness of this implementation. Conclusions and discussions are given in Section 5.

2. Orthogonal basis functions for moving least square interpolant

In the moving least square (MLS) interpolant, the function $u(\boldsymbol{x})$ is approximated [3] by

$$u^h(\boldsymbol{x}) = \sum_j^m p_j(\boldsymbol{x}) a_j(\boldsymbol{x}) \equiv \boldsymbol{p}^{\mathrm{t}}(\boldsymbol{x}) \boldsymbol{a}(\boldsymbol{x}) , \tag{1}$$

where $u^h(\boldsymbol{x})$ denotes the approximation of the function $u(\boldsymbol{x})$; $p_j(\boldsymbol{x})$ are m monomials in the space coordinates $\boldsymbol{x}^{\mathrm{t}} = [x, y]$ which are chosen so that the basis is complete. For example, in one dimension,

$$\boldsymbol{p}^{\mathrm{t}}(\boldsymbol{x}) = [1, x, x^2, \ldots, x^m] , \tag{2}$$

in two dimensions,

$$\boldsymbol{p}^{\mathrm{t}}(\boldsymbol{x}) = [1, x, y] \qquad \text{linear basis} \tag{3a}$$

$$\boldsymbol{p}^{\mathrm{t}}(\boldsymbol{x}) = [1, x, y, x^2, xy, y^2] \qquad \text{quadratic basis} \tag{3b}$$

$$\boldsymbol{p}^{\mathrm{t}}(\boldsymbol{x}) = [1, x, y, x^2, xy, y^2, x^3, x^2y, xy^2, y^3] \qquad \text{cubic basis} \tag{3c}$$

The coefficients $a_j(\boldsymbol{x})$ in (1) are functions of $\boldsymbol{x}$ and obtained by minimizing a weighted, discrete L_2 norm as follows:

$$J = \sum_I^n w(\boldsymbol{x} - \boldsymbol{x}_I)[\boldsymbol{p}^{\mathrm{t}}(\boldsymbol{x}_I)\boldsymbol{a}(\boldsymbol{x}) - u_I]^2 , \tag{4}$$

where n is the number of points in the neighborhood of $\boldsymbol{x}$ for which the weight function

$$w_I(\boldsymbol{x}) \equiv w(\boldsymbol{x} - \boldsymbol{x}_I) \neq 0 , \tag{5}$$

and u_I is the nodal value at $\boldsymbol{x} = \boldsymbol{x}_I$. Note that $u^h(\boldsymbol{x}_I) \neq u_I$. This neighborhood of $\boldsymbol{x}$ is called the domain of influence of $\boldsymbol{x}$, or circle of influence in two dimensions.

The stationarity of J in (4) with respect to $\boldsymbol{a}(\boldsymbol{x})$ leads to the following linear relation between $\boldsymbol{a}(\boldsymbol{x})$ and u_I:

$$\boldsymbol{A}(\boldsymbol{x})\boldsymbol{a}(\boldsymbol{x}) = \boldsymbol{B}(\boldsymbol{x})\boldsymbol{u} \tag{6a}$$

or

$$\boldsymbol{a}(\boldsymbol{x}) = \boldsymbol{A}^{-1}(\boldsymbol{x})\boldsymbol{B}(\boldsymbol{x})\boldsymbol{u} \tag{6b}$$

where $\boldsymbol{A}(\boldsymbol{x})$ and $\boldsymbol{B}(\boldsymbol{x})$ are defined by

$$\boldsymbol{A}(\boldsymbol{x}) = \sum_I^n w(\boldsymbol{x} - \boldsymbol{x}_I)\boldsymbol{p}(\boldsymbol{x}_I)\boldsymbol{p}^{\mathrm{t}}(\boldsymbol{x}_I) \tag{7a}$$

$$\boldsymbol{B}(\boldsymbol{x}) = [w(\boldsymbol{x} - \boldsymbol{x}_1)\boldsymbol{p}(\boldsymbol{x}_1), w(\boldsymbol{x} - \boldsymbol{x}_2)\boldsymbol{p}(\boldsymbol{x}_2), \ldots, w(\boldsymbol{x} - \boldsymbol{x}_n)\boldsymbol{p}(\boldsymbol{x}_n)] \tag{7b}$$

$$\boldsymbol{u}^{\mathrm{t}} = [u_1, u_2, \ldots, u_n] . \tag{7c}$$

As we mentioned before, (6) must be solved accurately to retain the accuracy of the MLS interpolant. When the matrix $\boldsymbol{A}(\boldsymbol{x})$ is not well-conditioned, (6) cannot be solved with the desired accuracy. However, the necessity for solving (6) can be eliminated by diagonalizing the matrix $\boldsymbol{A}(\boldsymbol{x})$.

To diagonalize the matrix $\boldsymbol{A}(\boldsymbol{x})$ for arbitrary $\boldsymbol{x}$, the following orthogonality condition is imposed at any point $\boldsymbol{x}$ where $\boldsymbol{a}(\boldsymbol{x})$ is to be computed:

$$\sum_I^n w(\boldsymbol{x} - \boldsymbol{x}_I) q_k(\boldsymbol{x}_I) q_i(\boldsymbol{x}_I) = 0 , \quad k \neq i . \tag{8}$$

To obtain the orthogonal basis functions $\boldsymbol{q}(\boldsymbol{x})$, it is necessary to distinguish the point at which we are evaluating $\boldsymbol{a}(\boldsymbol{x})$ from the dependence of the polynomial on $\boldsymbol{x}$. Let the point at which we are evaluating $\boldsymbol{a}(\boldsymbol{x})$ be denoted by $\bar{\boldsymbol{x}}$, and let the spatial variable be denoted by $\boldsymbol{x}$. Then the MLS interpolant is written

$$u^h(\boldsymbol{x}) = \sum_j^m q_j(\boldsymbol{x}, \bar{\boldsymbol{x}}) a_j(\bar{\boldsymbol{x}}) \equiv \boldsymbol{q}^{\mathrm{t}}(\boldsymbol{x}, \bar{\boldsymbol{x}})\boldsymbol{a}(\bar{\boldsymbol{x}}) , \tag{9}$$

where the basis functions $q_j(\boldsymbol{x}, \bar{\boldsymbol{x}})$ are constructed so that the following orthogonality condition is satisfied:

$$\sum_{I}^{n} w(x_I - \bar{x}) q_k(x_I, \bar{x}) q_j(x_I, \bar{x}) = 0 , \quad k \neq j . \tag{10}$$

For the given arbitrary basis functions $p_k(x)$ $(k = 1, \ldots, m)$, the orthogonal basis functions $q_k(x, \bar{x})$ can be obtained by using the Schmidt orthogonalization procedure as follows:

$$q_k(x, \bar{x}) = p_k(x) - \sum_{j}^{k-1} \alpha_{kj}(\bar{x}) q_j(x, \bar{x}) , \quad k = 1, \ldots, m , \tag{11}$$

where

$$\alpha_{kj}(\bar{x}) = \frac{\sum_{I}^{n} w_I(\bar{x}) p_k(x_I) q_j(x_I, \bar{x})}{\sum_{I}^{n} w_I(\bar{x}) q_j^2(x_I, \bar{x})} . \tag{12}$$

Using (2), the orthogonal basis functions $q_k(x, \bar{x})$ in one dimension can be given in the special form

$$q_1(x, \bar{x}) = 1 , \tag{13a}$$

$$q_2(x, \bar{x}) = x - \beta_1(\bar{x}) , \tag{13b}$$

$$q_{j+2}(x, \bar{x}) = (x - \beta_{j+1}(\bar{x})) q_{j+1}(x, \bar{x}) - \gamma_j(\bar{x}) q_j(x, \bar{x}) , \quad j = 1, \ldots, m-2 , \tag{13c}$$

where

$$\beta_{j+1}(\bar{x}) = \frac{\sum_{I}^{n} w_I(\bar{x}) x_I q_{j+1}^2(x_I, \bar{x})}{\sum_{I}^{n} w_I(\bar{x}) q_{j+1}^2(x_I, \bar{x})} , \quad j = 0, \ldots, m-2 , \tag{14a}$$

$$\gamma_j(\bar{x}) = \frac{\sum_{I}^{n} w_I(\bar{x}) q_{j+1}^2(x_I, \bar{x})}{\sum_{I}^{n} w_I(\bar{x}) q_j^2(x_I, \bar{x})} , \qquad j = 1, \ldots, m-2 . \tag{14b}$$

Because of the orthogonality condition (10), the matrix A becomes diagonal and the coefficients $a_j(\bar{x})$ can be directly obtained from (6):

$$a_j(\bar{x}) = \frac{\sum_{I}^{n} w_I(\bar{x}) q_j(x_I, \bar{x}) u_I}{b_j(\bar{x})} , \quad j = 1, \ldots, m , \tag{15a}$$

and

$$b_j(\bar{x}) = \sum_{J}^{n} w_J(\bar{x}) q_j^2(x_J, \bar{x}) . \tag{15b}$$

The distinction between x and $\bar{x}$ is only needed in the least square minimization. Once this is completed, the coefficients are determined at a point x, the distinction between x and $\bar{x}$ is no longer necessary, so we can replace the variable $\bar{x}$ by x in (9) and (15). Thus, the MLS interpolant approximation can be written as follows:

$$u^h(x) = \sum_{I}^{n} \phi_I(x) u_I , \tag{16}$$

where the shape function $\phi_I(x)$ is defined by

$$\phi_I(x) = w_I(x) \sum_{j}^{m} C_{jI}(x) , \tag{17a}$$

$$C_{jI}(x) = \frac{q_j(x, x) q_j(x_I, x)}{b_j(x)} . \tag{17b}$$

The partial derivatives of $\phi_I(x)$ can be obtained as follows:

$$\phi_{I,k}(x) = w_{I,k}(x) \sum_j^m C_{jI}(x) + w_I(x) \sum_j^m C_{jI,k}(x) , \tag{18}$$

where

$$C_{jI,k}(x) = [q_{j,k}(x,x)q_j(x_I,x) + q_j(x,x)q_{j,k}(x_I,x) - b_{j,k}(x)C_{jI}(x)]/b_j(x) , \tag{19a}$$

$$b_{j,k}(x) = \sum_J^n [w_{J,k}(x)q_j^2(x_J,x) + 2w_J(x)q_j(x_J,x)q_{j,k}(x_J,x)] , \tag{19b}$$

where the index k following a comma denotes derivative with respect to x_k.

The advantage of using orthogonal basis functions is that it not only reduces the computational cost but also improves the accuracy of interpolates when the condition number of matrix A is very small. It should be noted that (17) and (19) also hold for three-dimensional problems.

3. Modified variational principle and numerical implementation

3.1. Variational principle

We consider the two-dimensional problem with small displacements on the domain Ω bounded by Γ. The equilibrium equation is

$$\nabla \cdot \boldsymbol{\sigma} + \boldsymbol{b} = \boldsymbol{0} \quad \text{in } \Omega , \tag{20}$$

where $\boldsymbol{\sigma}$ is the stress tensor, which corresponds to the displacement field $\boldsymbol{u}$; $\boldsymbol{b}$ is a body force vector. The boundary conditions are given as follows:

$$\boldsymbol{\sigma} \cdot \boldsymbol{n} = \bar{\boldsymbol{t}} \quad \text{on } \Gamma_t , \tag{21a}$$

$$\boldsymbol{u} = \bar{\boldsymbol{u}} \quad \text{on } \Gamma_u , \tag{21b}$$

in which the superposed bar denotes prescribed boundary values, and $\boldsymbol{n}$ is the unit normal to the domain Ω.

The variational (or weak) form of the equilibrium equation is posed as follows. Let test functions $\delta \boldsymbol{v}(x) \in H^1$ and $\delta \boldsymbol{\lambda}(x) \in H^0$, consider trial functions $\boldsymbol{u}(x) \in H^1$ and Lagrange multipliers $\boldsymbol{\lambda}(x) \in H^0$. Then if

$$\int_\Omega \nabla_s \delta \boldsymbol{v} : \boldsymbol{\sigma} \, d\Omega - \int_\Omega \delta \boldsymbol{v} \cdot \boldsymbol{b} \, d\Omega - \int_{\Gamma_t} \delta \boldsymbol{v} \cdot \bar{\boldsymbol{t}} \, d\Gamma - \int_{\Gamma_u} \delta \boldsymbol{\lambda} \cdot (\boldsymbol{u} - \bar{\boldsymbol{u}}) \, d\Gamma$$

$$- \int_{\Gamma_u} \delta \boldsymbol{v} \cdot \boldsymbol{\lambda} \, d\Gamma = 0 \quad \forall \delta \boldsymbol{v} \in H^1, \ \delta \boldsymbol{\lambda} \in H^0 , \tag{22}$$

then (20), (21a) and (21b) are satisfied. In the above, $\nabla_s \boldsymbol{v}$ is the symmetric part of $\nabla \boldsymbol{v}$; H^1 and H^0 denote the Sobolev spaces of degree one and zero, respectively. Note that the trial functions do not satisfy the essential boundary conditions, so that they are imposed by Lagrange multipliers.

To obtain a modified variational principle, we integrate the first term on the left side of (22) by parts

$$\int_\Gamma \delta \boldsymbol{v} \cdot \boldsymbol{t} \, d\Gamma - \int_\Omega \delta \boldsymbol{v} \cdot (\nabla \cdot \boldsymbol{\sigma} + \boldsymbol{b}) \, d\Omega - \int_{\Gamma_t} \delta \boldsymbol{v} \cdot \bar{\boldsymbol{t}} \, d\Gamma - \int_{\Gamma_u} \delta \boldsymbol{\lambda} \cdot (\boldsymbol{u} - \bar{\boldsymbol{u}}) \, d\Gamma - \int_{\Gamma_u} \delta \boldsymbol{v} \cdot \boldsymbol{\lambda} \, d\Gamma = 0 , \tag{23a}$$

or

$$- \int_\Omega \delta \boldsymbol{v} \cdot (\nabla \cdot \boldsymbol{\sigma} + \boldsymbol{b}) \, d\Omega - \int_{\Gamma_t} \delta \boldsymbol{v} \cdot (\bar{\boldsymbol{t}} - \boldsymbol{t}) \, d\Gamma - \int_{\Gamma_u} \delta \boldsymbol{\lambda} \cdot (\boldsymbol{u} - \bar{\boldsymbol{u}}) \, d\Gamma - \int_{\Gamma_u} \delta \boldsymbol{v} \cdot (\boldsymbol{\lambda} - \boldsymbol{t}) \, d\Gamma = 0 , \tag{23b}$$

where $\boldsymbol{t} = \boldsymbol{\sigma} \cdot \boldsymbol{n}$ is the traction along the boundary. It can be seen from the above equation that for all

variations $\delta \boldsymbol{v}$ and $\delta \boldsymbol{\lambda}$, the first term on the left side gives the equilibrium equation, the second term the natural boundary condition on Γ_t and the third term the essential boundary condition on Γ_u. The last term on the left side of (23b) must vanish for all variation $\delta \boldsymbol{v}$ which requires

$$\boldsymbol{\lambda} = \boldsymbol{t} \quad \text{on } \Gamma_u , \tag{24}$$

i.e., the physical meaning of the Lagrange multipliers $\boldsymbol{\lambda}$ is the traction along the boundary Γ_u. Therefore, substituting (24) into (22) yields a modified variational principle [5, 6].

$$\int_\Omega \nabla_s \delta \boldsymbol{v} : \boldsymbol{\sigma} \, \mathrm{d}\Omega - \int_\Omega \delta \boldsymbol{v} \cdot \boldsymbol{b} \, \mathrm{d}\Omega - \int_{\Gamma_t} \delta \boldsymbol{v} \cdot \bar{\boldsymbol{t}} \, \mathrm{d}\Gamma - \int_{\Gamma_u} \delta \boldsymbol{t} \cdot (\boldsymbol{u} - \bar{\boldsymbol{u}}) \, \mathrm{d}\Gamma - \int_{\Gamma_u} \delta \boldsymbol{v} \cdot \boldsymbol{t} \, \mathrm{d}\Gamma = 0 . \tag{25}$$

3.2. Discrete equations

We now consider linear elasticity where

$$\boldsymbol{\varepsilon} = \nabla_s \boldsymbol{u} , \qquad \boldsymbol{\sigma} = \boldsymbol{D}\boldsymbol{\varepsilon} . \tag{26a,b}$$

In order to obtain the discrete equation from the weak form (25), the approximate solution $\boldsymbol{u}$ and the test function $\boldsymbol{v}$ are constructed according to (16). The final discrete equations can be obtained by substituting the trial functions and test functions into the weak form (25), which yields

$$\boldsymbol{K}\boldsymbol{u} = \boldsymbol{f} \tag{27a}$$

and $\boldsymbol{K}$ and $\boldsymbol{f}$ consist of 2×2 submatrices $\boldsymbol{K}_{IJ}$ and 2×1 submatrices $\boldsymbol{f}_I$ given by

$$\boldsymbol{K}_{IJ} = \int_\Omega \boldsymbol{B}_I^{\mathrm{t}} \boldsymbol{D} \boldsymbol{B}_J \, \mathrm{d}\Omega - \int_{\Gamma_u} \phi_I \boldsymbol{S} \boldsymbol{N} \boldsymbol{D} \boldsymbol{B}_J \, \mathrm{d}\Gamma - \int_{\Gamma_u} \boldsymbol{B}_I^{\mathrm{t}} \boldsymbol{D}^{\mathrm{t}} \boldsymbol{N}^{\mathrm{t}} \boldsymbol{S} \phi_J \, \mathrm{d}\Gamma , \tag{27b}$$

$$\boldsymbol{f}_I = \int_{\Gamma_t} \phi_I \bar{\boldsymbol{t}} \, \mathrm{d}\Gamma + \int_\Omega \phi_I \boldsymbol{b} \, \mathrm{d}\Omega + \int_{\Gamma_u} \boldsymbol{B}_I^{\mathrm{t}} \boldsymbol{D}^{\mathrm{t}} \boldsymbol{N}^{\mathrm{t}} \boldsymbol{S} \bar{\boldsymbol{u}} \, \mathrm{d}\Gamma , \tag{27c}$$

where

$$\boldsymbol{D} = \frac{E}{1-\nu^2} \begin{bmatrix} 1 & \nu & 0 \\ \nu & 1 & 0 \\ 0 & 0 & (1-\nu)/2 \end{bmatrix} \quad \text{for plane stress} , \tag{28}$$

$$\boldsymbol{B}_I = \begin{bmatrix} \phi_{I,x} & 0 \\ 0 & \phi_{I,y} \\ \phi_{I,y} & \phi_{I,x} \end{bmatrix} , \tag{29b}$$

$$\boldsymbol{N} = \begin{bmatrix} n_x & 0 & n_y \\ 0 & n_y & n_x \end{bmatrix} , \tag{29b}$$

$$\boldsymbol{S} = \begin{bmatrix} s_x & 0 \\ 0 & s_y \end{bmatrix} , \tag{29c}$$

and

$$s_x = \begin{cases} 1 , & \text{if prescribed } u_x \text{ on } \Gamma_u , \\ 0 , & \text{if prescribed } u_y \text{ on } \Gamma_u , \end{cases} \tag{30a}$$

$$s_y = \begin{cases} 0 , & \text{if prescribed } u_x \text{ on } \Gamma_u , \\ 1 , & \text{if prescribed } u_y \text{ on } \Gamma_u , \end{cases} \tag{30b}$$

in which E and ν are Young's modulus and Poisson's ratio, respectively. Note that the coefficient matrix in (27b) is symmetric and banded.

3.3. Weight function

In all numerical examples presented in this paper, the exponential weight function with $k = 1$ given in [2] is used, which is

$$w_I(d_I^{2k}) = \begin{cases} \dfrac{e^{-(d_I/c)^{2k}} - e^{-(d_{mI}/c)^{2k}}}{(1 - e^{-(d_{mI}/c)^{2k}})}, & \text{if } d_I \leq d_{mI}, \\ 0, & \text{if } d_I > d_{mI}, \end{cases} \tag{31a}$$

$$d_I = \|\boldsymbol{x} - \boldsymbol{x}_I\| \tag{31b}$$

where c is a constant which controls the relative weight; d_{mI} is the domain of the support for the weight function $w_I(d_I^{2k})$. This domain, where $w_I(\boldsymbol{x})$ is nonzero, is often called the domain of influence of node $\boldsymbol{x}_I$. It was shown in [2] that the derivatives of the above weight function with respect to x or y exist to any desired order if k is a positive integer. Moreover, it was found in the above that the above weight function, which is essentially a truncated Gauss distribution, performs far better than a conical weight function. In the latter, the results are more sensitive to the value of d_{mI}.

Note that the definition of c is more or less arbitrary. We will use the definition given in [2] as follows:

$$c = \alpha c_I, \tag{32a}$$

where

$$c_I = \max_{J \in S_J} \|\boldsymbol{x}_J - \boldsymbol{x}_I\|. \tag{32b}$$

We have used $1 \leq \alpha \leq 2$, and used α near 1 for problems with singularities and high gradients. In the above, S_J is the minimum set of neighboring points of $\boldsymbol{x}_I$ which construct a polygon surrounding $\boldsymbol{x}_I$. If the nodes are uniformly distributed, then c_I in (32b) is the maximum distance between nodes. In the case where the nodes are randomly distributed but the integration cells are uniformly distributed, c_I can be defined as a characteristic length of integration zone (or cell) that contains the point $\boldsymbol{x}_I$.

3.4. Numerical implementation

In order to perform the integrations in (27), the quadrature scheme with a cell structure proposed in [2] is used. The cells are independent of the nodes and are arranged in a regular pattern in both dimensions as shown in Fig. 1.

The organization of the program is similar to that of finite element programs as shown in Table 1. In forming the equations, each cell is considered in turn and Gaussian quadrature is performed. To perform the quadrature, the domain of influence of each quadrature point must be determined. The domains of influence of two typical points is also shown in Fig. 1. As can be seen, the domain of influence of a point never extends across any boundaries. Thus, for a quadrature point next to a crack,

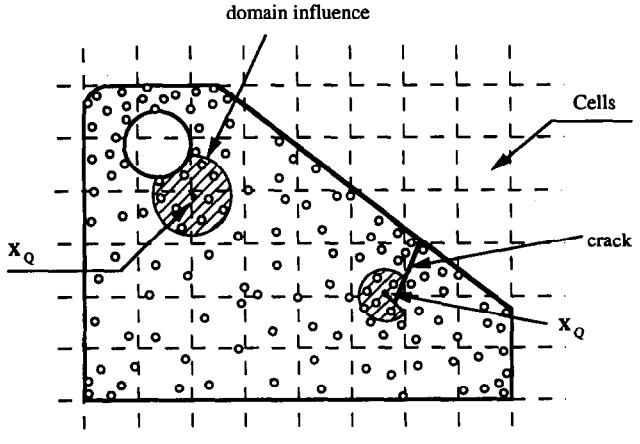

Fig. 1. Cell structure for quadrature in the EFG method and domains of influence of two quadrature points as shown.

Table 1
Flowchart for construction of equations in EFG

1. **loop** over cells of domain C
   2. **loop** over quadrature points x_Q in cell C
   (a) if quadrature point outside physical domain, go to 2(g);
   (b) check all nodes in cell and surrounding cells to determine the m nodes x_I, $I=1$ to m in the domain of influence of x_Q;
   (c) if a boundary segment exists in the cell around cell C and if $x-x_Q$ intersects the boundary segment, go to 2(g);
   (d) compute $\phi_I(x_Q)$ and $\phi_{I,i}(x_Q)$ at the quadrature point;
   (e) evaluate contributions to (29);
   (f) assemble contributions to nodes;
   (g) end if.
   3. **end** quadrature point loop
4. **end** cell loop
5. solve governing equations $\boldsymbol{Kd}=\boldsymbol{f}$
6. post-process to compute strains and stresses.

the domain of influence of x_Q is limited to those points x_I which can be connected to x_Q without intersecting the crack.

The contributions of a quadrature point to the linear equations depends on the nodes in the domain of influence on the point x_Q. Each quadrature point contributes nonzero entries to the equations only to those nodes which are in its domain of influence. Thus, in the final equations, no coupling occurs between nodes which are not within a specified distance (which corresponds to the domain of influence) and the corresponding entries in $\boldsymbol{K}$ vanish. If the nodes are numbered judiciously, for example by sorting the x-coordinates, the equations will be banded.

The check in step 2(c) in Table 1 is necessary to correctly deal with interior boundaries such as cracks and holes. As shown in the lower right hand corner of the example in Fig. 1, the domain of influence of a point does not extend across a boundary adjacent to that point. Thus, only those points x_I which can be connected to x_Q without intersecting any boundary are in the domain of influence of x_Q. In each cell, Gauss quadrature is used. The number of quadrature points depends on the number of nodes in a cell. We have used $n_Q \times n_Q$ Gauss quadrature in each cell with $n_Q = \sqrt{m} + 3$, where m is the number of nodes in a cell.

4. Numerical results

4.1. Path test

The first numerical example is the standard patch test, shown in Fig. 1. In this patch test, the displacements are prescribed on all outside boundaries by a linear function of x and y on a patch of dimension $L_x = 2$ by $L_y = 2$ with displacements of order 1. Satisfaction of the patch test then requires that the displacement of any interior nodes be given by the same linear function and that the strains and stresses be constant in the patch.

We use $c = c_I$ and $d_{mI} = 4c$ in the calculation. The EFG method with the present formulation exactly passes all patch tests shown in Fig. 2(a)–(c). Note that for the patch test (b), four cells with the dimension $L_x/2$ by $L_y/2$ were used and the nodes which construct the cells were also used as the data points in the calculation of the EFG method. To illustrate the importance of imposing the essential boundary conditions, Table 1 gives the errors in the L_2-norm of the displacement when the essential boundary conditions are imposed by setting the nodal values of $\boldsymbol{u}_I$ to the prescribed values. This approach fails to satisfy the essential boundary conditions exactly because the MLS interpolants $\phi_I(x)$ do not satisfy the property $\phi_I(x_J) = \delta_{IJ}$ and they do not vanish along the entire boundary even when they vanish at nodes. As can be seen from Table 2, the resulting errors in the solution are quite large.

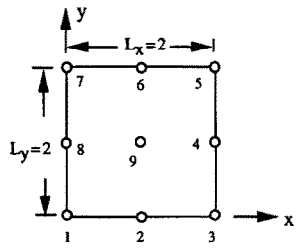

(a) EFG with regular nodes

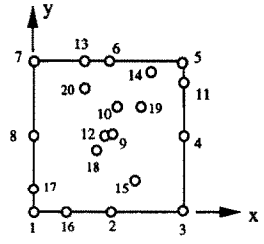

(b) EFG nodes as shown in Table

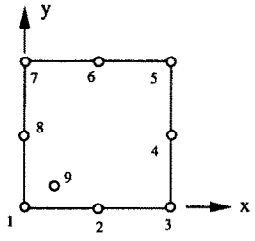

(c) EFG with irregular node 9

Coordinates for patch (b)

node	coordinate (x,y)
16	0.3, 0.
17	0., 0.2
15	1.2, 0.4
18	0.8, 0.9
12	0.9, 1.
19	1.4, 1.2
20	0.5, 1.3
10	1.1, 1.2
11	2., 1.8
13	0.8, 2.
14	1.6, 1.9

Fig. 2. Nodes used in the EFG method for patch tests.

4.2. Beam

The behavior of the present formulation of the EFG method was also studied in the cantilever beam problem, for which the following exact solution is given in [7]:

$$u_x = \frac{P}{6\bar{E}I}\left(y - \frac{D}{2}\right)\left[(6L - 3x)x + (2 + \bar{\nu})(y^2 - 2Dy)\right], \tag{33a}$$

$$u_y = \frac{P}{6\bar{E}I}\left[3\bar{\nu}\left(y^2 - 2Dy + \frac{D^2}{2}\right)(L - x) + \frac{1}{4}(4 + 5\bar{\nu})D^2x + \left(L - \frac{x}{3}\right)3x^2\right], \tag{33b}$$

where

$$I = \frac{D^3}{12}, \tag{34a}$$

$$\bar{E} = \begin{cases} E, & \text{for plane stress}, \\ E/(1 - \bar{\nu}^2), & \text{for plane strain}, \end{cases} \tag{34b}$$

Table 2
Relative error in L_2 norm $\|u^h - u\|/\|u\|$ for patch test

	EFG (present formulation)	EFG (essential BC imposed by prescribed nodal values)
Mesh (a)	0.0	0.01262
Mesh (b)	0.0	0.45373
Mesh (c) nodal 9 located (0.9, 0.9)	0.0	0.01262
Mesh (c) nodal 9 located (0.3, 0.4)	0.0	0.24929

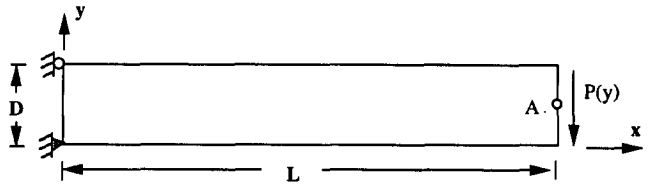

a). Cantilever beam

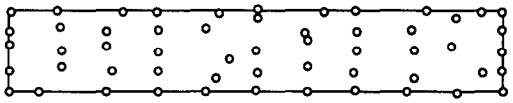

b). data points for EFG

Fig. 3. Description of the beam problem and nodal points used in EFG.

$$\bar{\nu} = \begin{cases} \nu\,, & \text{for plane stress}\,, \\ \nu/(1-\nu)\,, & \text{for plane strain}\,. \end{cases} \tag{34c}$$

The stresses corresponding to (33) are

$$\sigma_x(x, y) = -\frac{P}{I}(L-x)\left(y - \frac{D}{2}\right), \tag{35a}$$

$$\sigma_y(x, y) = 0\,, \tag{35b}$$

$$\sigma_{xy}(x, y) = -\frac{Py}{2I}(y - D)\,. \tag{35c}$$

Tractions corresponding to (35) were applied on the end $x = L$ and displacements corresponding to (33) at $x = 0$. The problem was solved for the plane strain case with $E = 3.0 \times 10^7$, $D = 1$ and $L = 8$. The irregular mesh of nodes shown in Fig. 3 was considered. The cell arrangement consists of four zones in the vertical direction, ten zones in the horizontal direction. In each cell, 5 by 5 Gauss quadrature was used to evaluate the stiffness of the EFG. EFG solutions were obtained with orthogonal forms of linear, quadratic and cubic basis functions using the same nodes; see (3) for definitions of the linear, quadratic and cubic basis functions.

The deflection at point A, w^{NUM}, is compared to the analytical result w^{EXACT} in Table 3 with $\alpha = 2$ and $d_{mI} = 4c$. For comparison, finite element solutions were also obtained using the standard 4-node quadrilateral with full 2×2 Gauss quadrature, Q4, and a mixed element QBI [8]. In the latter, the higher order terms in the strain field were constructed so that locking is avoided for nearly incompressible materials and convergence is enhanced for beam bending.

Table 3
Tip-deflection ratio for the beam problem using present formulas

	$w^{\mathrm{NUM}}/w^{\mathrm{EXACT}}$ at Point A	
Method	Case 1 plane strain $\nu = 0.25$	Case 2 plane strain $\nu = 0.4999$
FEM: Q4	0.607	0.029
FEM: QBI	0.745	0.683
EFG: linear	0.999	0.999
EFG: quadratic	1.000	1.000
EFG: cubic	1.000	1.000

In this new implementation, as in the previous implementation in [2], the EFG results do not exhibit any locking, even though no modifications were made in the nearly incompressible case, $\nu = 0.4999$ in plane strain. Note that the Q4 element locks in this situation. The EFG method, if anything, is somewhat flexible.

Figure 4 shows the shear stress σ_{xy} and normal stress σ_x for $\nu = 0.25$ at $x = L/2$ obtained by the EFG method with linear basis functions. The solution obtained by QBI is also included. Note that the stresses from the finite element solution are not continuous along the line $x = L/2$. The discontinuous stress σ_{xy} is denoted as σ_{xy} (+) in the right element and σ_{xy} (−) in the left element in Fig. 4. For comparison, the result obtained using the formulations given in [2] are also given in Fig. 4 and denoted as EFG-LM, i.e., the element free Galerkin implementation in which Lagrange multipliers (LM) are used to impose the essential boundary conditions. It can be seen that the stress field obtained by EFG is much better than that obtained by FEM. It is noted from Fig. 4 that the EFG solution satisfies the traction free boundary conditions (at $y = 0$ and $y = 1$) very well.

4.3. *Hole in an infinite plate*

This problem is a portion of an infinite plate with a central circular hole subjected to a unidirectional tensile load of 1.0 in the x direction as shown in Fig. 5. Due to symmetry, only the upper right quadrant of the plate is modeled. Plane strain conditions were assumed with $E = 1.0 \times 10^3$ and $\nu = 0.3$. Symmetry

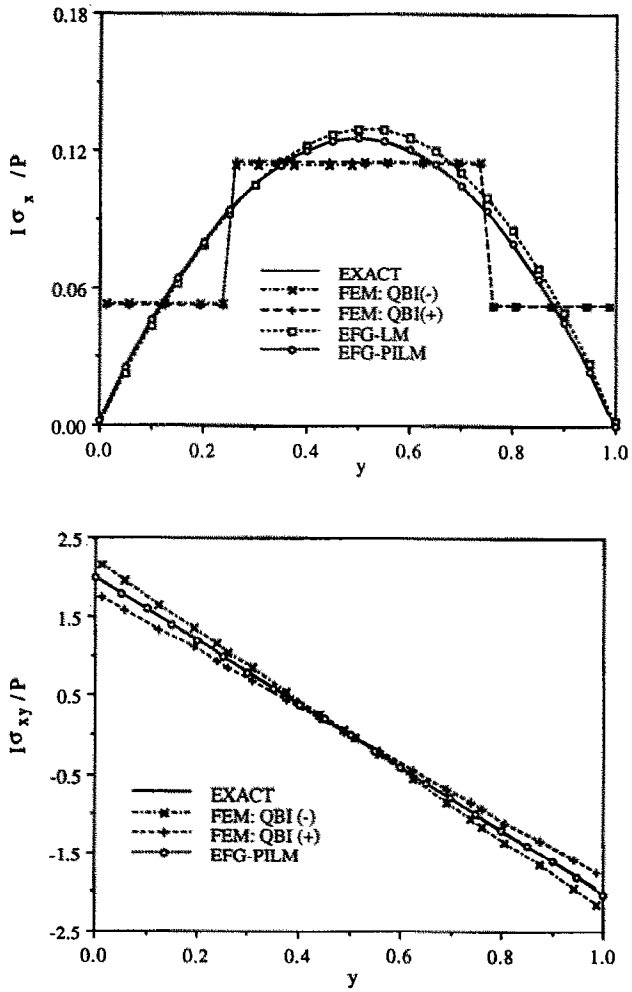

Fig. 4. Stresses at $x = L/2$ for $\nu = 0.25$ in the beam problem; PILM is the new method presented here.

conditions were imposed on the left and bottom edges, and the inner boundary of the hole is traction free. The exact solution for the stresses is

$$\sigma_x(x, y) = 1 - \frac{a^2}{r^2}\{\tfrac{3}{2}\cos 2\theta + \cos 4\theta\} + \frac{3a^4}{2r^4}\cos 4\theta\,, \tag{36a}$$

$$\sigma_y(x, y) = -\frac{a^2}{r^2}\{\tfrac{1}{2}\cos 2\theta - \cos 4\theta\} - \frac{3a^4}{2r^4}\cos 4\theta\,, \tag{36b}$$

$$\sigma_{xy}(x, y) = -\frac{a^2}{r^2}\{\tfrac{1}{2}\sin 2\theta + \sin 4\theta\} + \frac{3a^4}{2r^4}\sin 4\theta\,, \tag{36c}$$

where (r, θ) are the usual polar coordinates and θ is measured from the positive x axis counter-clockwise. Traction boundary conditions given by the exact solution (36) were imposed on the right ($x = 5$) and top ($y = 5$) edges.

The initial mesh of 54 nodes is shown in Fig. 5(a). Subsequently, the number of nodes was increased to 139 as shown in Fig. 5(d). We use $c = c_I$ and $d_{mI} = 4c$ in the calculation. The stress σ_x at $x = 0$ obtained by the EFG method is given in Fig. 6. The result using only the nodes in Fig. 5(a) is also shown in Fig. 6 for comparison.

The relative accuracy of this implementation of the EFG method with the Lagrange multiplier form was further studied by examining convergence in various error norms. Figures 7 and 8 compare the L_2-norm of the errors in displacements and energy norm of the new method with the Lagrange multiplier form for the beam problem. Figure 9 compares the energy norms for the error for the hole problem. As can be seen, the Lagrange multiplier implementation is more accurate, but the accuracy can be equaled by the new implementation by adding approximately 25–50% more nodes for this range of unknowns. Note that the LM method would have more unknowns because of the additional

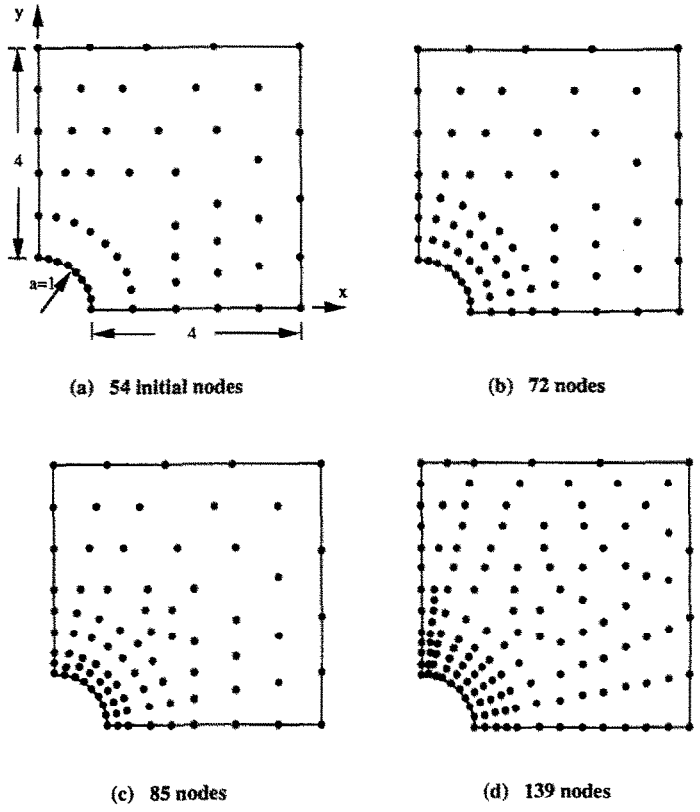

Fig. 5. Meshes for a square plate as a portion of an infinite plate with a central circular hole subjected to a unidirectional tensile load of 1.0 in the x direction.

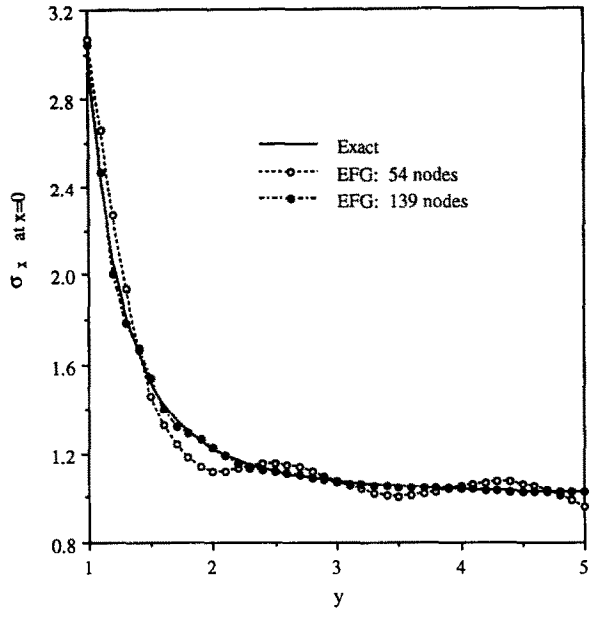

Fig. 6. Comparison between the exact solution in the EFG results for stresses σ_x at $x = 0$.

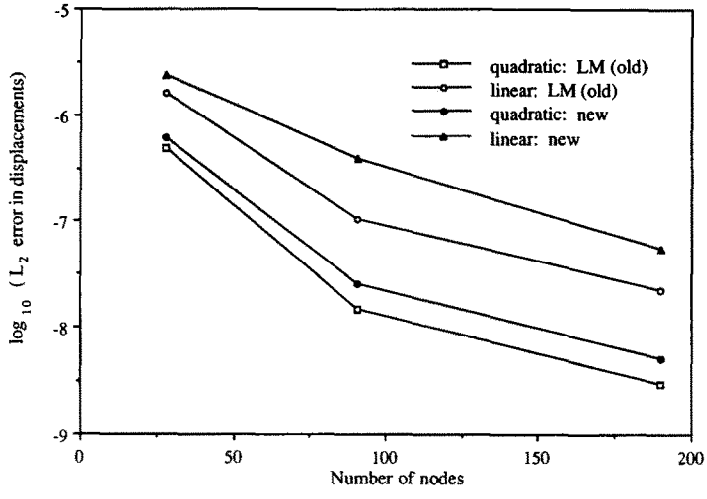

Fig. 7. Convergence of displacements in L_2 norm for the beam problem.

Lagrange multipliers. The relative accuracy of the LM form decreases with an increasing number of nodes. We have not used an optimal solver for the Lagrange multiplier form of the equations, but currently we can achieve the equivalent accuracy with the new implementation at about 50% of the cost.

4.4. *Edge crack*

A rectangular plate with an edge crack of length $a/w = 0.5$ is shown in Fig. 10. Twofold symmetry was used. The node arrangement consists of a set of uniformly spaced nodes combined with the four different patterns around the crack tip shown in Fig. 11. The mode I stress intensity factor K_I was evaluated by using the J integral which was converted into the domain integral by using Green's theorem [9–11]. The number of cells was 10×10, and 5×5 Gauss quadrature was used in all cells

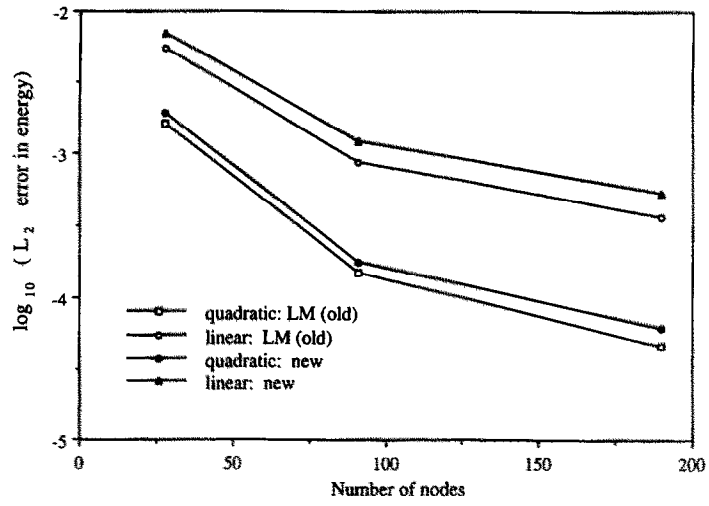

Fig. 8. Convergence in energy norm for the beam problem.

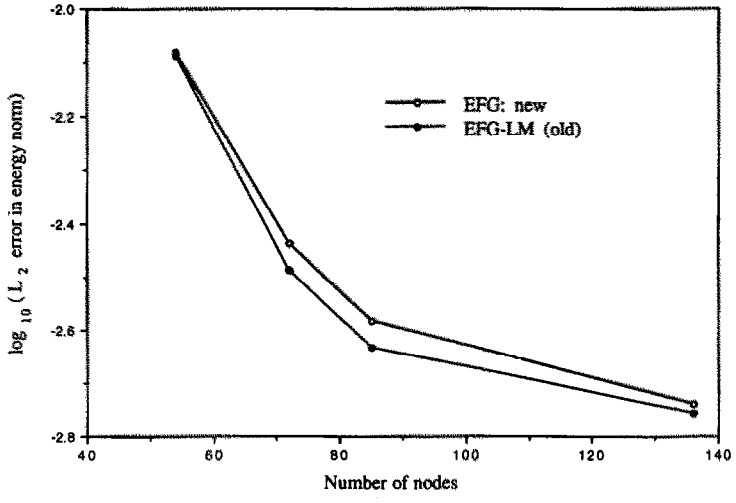

Fig. 9. Convergence in energy norm for the hole problem in an infinite plate.

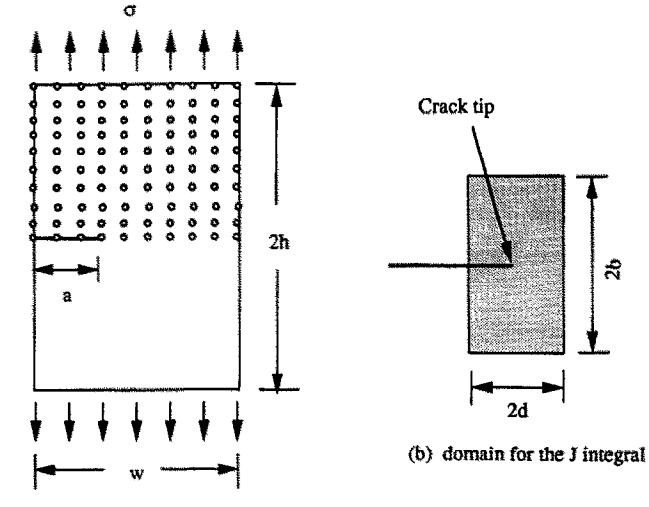

Fig. 10. Problem statement for a single edge cracked plate.

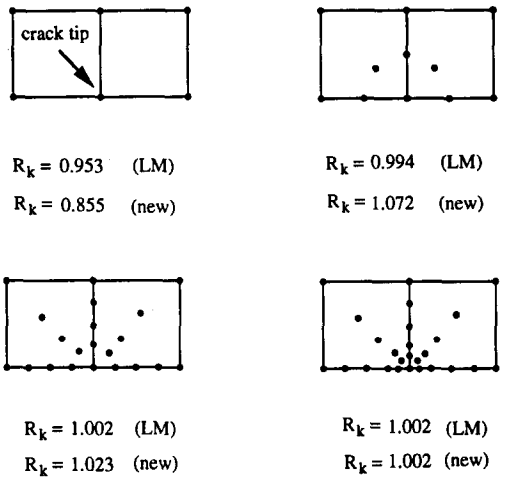

Fig. 11. Node point arrangements and results for the edge crack problem. Stress intensity $R_k = K_I/K_{exact}$ factors are obtained by using the J-integral over a rectangular domain with $b/d = 2$ and $d = 0.8a$ centered on the crack tip shown in Fig. 10.

except the two around the crack tip, where 9×9 Gauss quadrature was used. Linear basis functions were used.

Normalized values of K_I for the various nodal arrangements about the crack tip are shown in Fig. 11. Again, while the LM method is significantly more accurate for coarse meshes, for the finest mesh the new method has comparable accuracy; both methods are with 0.2% of the benchmark solution of Tada et al. [12]. Note that the method easily enables meshes designed to reflect the overall geometry to be combined with a local mesh designed to capture an accurate approximation to the singular stress field at the crack tip.

Figure 12 shows two meshes which were used to model the progressive growth of the crack. The meshes were constructed by simply translating the dense pattern shown in Fig. 11(d) through the fixed mesh representing the geometry, dividing any nodes which have been passed by the crack into two and displacing their normal to the crack surface by a distance $10^{-4}w$. The nodes need to be moved a small distance only to guarantee that their occurrence in the domain of influence of adjoining points is correctly identified in step 2(c) of the flowchart.

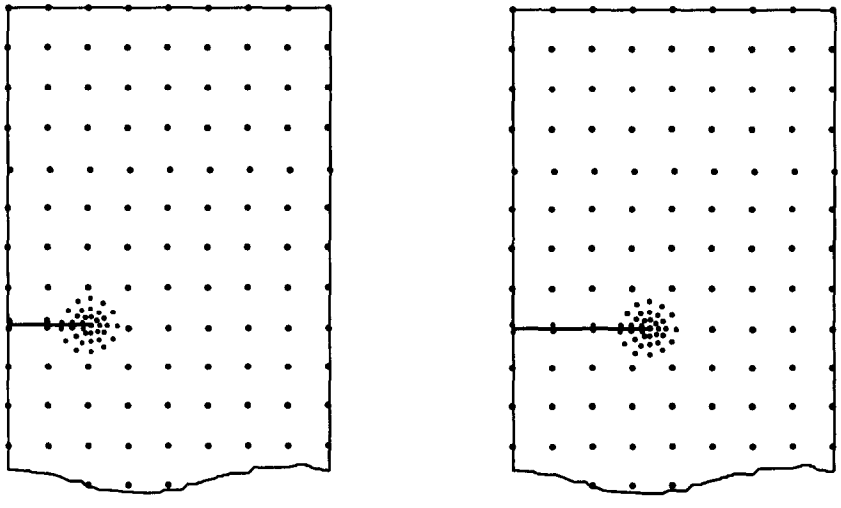

Fig. 12. Two meshes for the progressive growth of the edge crack problem.

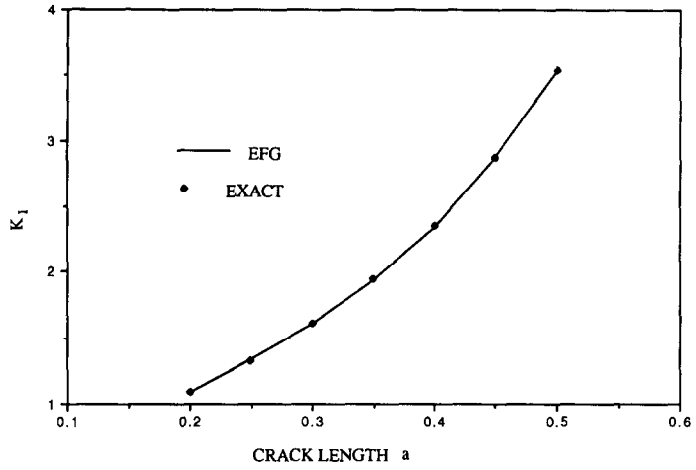

Fig. 13. Stress intensity factors for the edge crack problem.

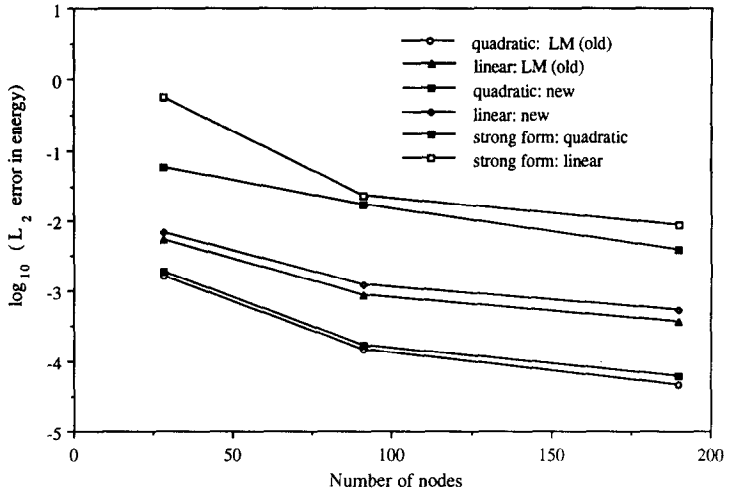

Fig. 14. Convergence in energy norm for the beam problem.

The value of the mode I stress intensity factor as a function of the crack length is given in Fig. 13. As can be seen, the computed stress intensity factor agrees closely with the benchmark value in [12] for all values of the crack length. Thus, the computation of K_I in the EFG method is not detrimentally affected by irregularities in the mesh arrangement as the nodes around the crack tip are moved through the fixed mesh of nodes.

4.5. Strong form

As a minor side issue, we consider the performance of MLS interpolants with an implementation of the strong form, where (20) and (21) are imposed directly at each node. To assess the performance, we solved the beam problem with three meshes. Figure 14 shows the error in the energy norm for these three solutions for the strong form and two implementations of EFG with both linear and quadratic basis functions. As can be seen, the strong form is strikingly less accurate. This is not unexpected, since in a direct implementation of the strong form, it can only be imposed at nodes, whereas the Galerkin method minimizes error over the set of all quadrature points. The performance of a strong form would probably improve if it were enforced in an integral sense, but then the method has significant disadvantages (the need for higher derivatives) but no advantages.

5. Conclusions

A new approach to implement the element free Galerkin method (EFGM) has been proposed. It features the following:

(1) orthogonal MLS interpolants are constructed so that matrix inversion at each quadrature point is avoided;
(2) essential boundary conditions are imposed through a modified variational principle so that the use of Lagrange multipliers is avoided.

The latter provides discrete equations which are banded and positive definite, which is a significant advantage. Although for a given number of nodes the new form is slightly less accurate, the loss of accuracy diminishes with increasing numbers of unknowns. For a reasonable number of nodes, the new method almost equals the accuracy of the EFG method with Lagrange multipliers without engendering the disadvantages of the latter in the structure of the discrete equations.

The results presented in these studies show significant advantages for the EFG method over the finite element Galerkin method:

(1) the method is significantly more accurate than the finite element method for elliptic PDEs even when linear basis functions are used;
(2) the method provides smooth solutions for strains and stresses;
(3) the method avoids volumetric locking for nearly incompressible materials without any modifications.

These advantages were also noted in [2]. The results presented here show that the EFG method is particularly effective in progressive fracture problems because it can accurately compute stress intensity factors with very irregular arrangements of nodes. Therefore it is possible to move a dense arrangement of nodes around a crack tip, which effectively captures the stress singularity and the stress intensity factors, through another stationary arrangement which reflects the geometry. Thus the burdens of continuous remeshing which make the treatment of progressive fracture by finite element methods very burdensome are avoided.

While the boundary element method also can avoid extensive remeshing, the EFG method has the following advantages over the boundary element method:

(1) the discrete equations are sparse, banded, symmetric and more well-conditioned;
(2) it is applicable to anisotropic materials and other complex constitutive laws;
(3) it is readily applicable to nonlinear problems and other complex constitutive laws because it does no require a Green's function;
(4) it can easily be extended to shells.

Thus while the EFG method is attractive in many problems because of the simplicity of meshing (only nodes and boundaries are needed) and post-processing (results are already smooth), its strongest appeal is in problems such as progressive fractur.

Acknowledgment

The support of the National Science Foundation and U.S. Air Force Office of Scientific Research to Northwestern University is gratefully acknowledged.

References

[1] B. Nayroles, G. Touzot and P. Villon, Generalizing the finite element method: diffuse approximation and diffuse elements, Comput. Mech. 10 (1992) 307–318.
[2] T. Belytschko, Y.Y. Lu and L. Gu, Element free Galerkin methods, Internat. J. Numer. Methods and Engrg., in press.
[3] P. Lancaster and K. Salkauskas, Surfaces generated by moving least squares methods, Math. Comp. 37 (1981) 141–158.
[4] D. Shepard, A two-dimensional interpolation function for irregularly spaced points, Proc. A.C.M. Natl. Conf. (1968) 517–524.
[5] K. Washizu, Variational Methods in Elasticity and Plasticity, 2nd edition (Pergamon, New York, 1975).

[6] O.C. Zienkiewicz and K. Morgan, Finite Elements and Approximation (Wiley, New York, 1983).
[7] S.P. Timoshenko and J.N. Goodier, Theory of Elasticity, 3rd edition (McGraw-Hill, New York, 1970).
[8] T. Belytschko and W.E. Bachrach, Efficient implementation of quadrilaterals with high coarse-mesh accuracy, Comput. Methods Appl. Mech. Engrg. 54 (1986) 279–301.
[9] F.Z. Li, C.F. Shih and A. Needleman, A comparison of methods for calculating energy release rates, Engrg. Fract. Mech. 21 (1985) 405–421.
[10] B. Moran and C.F. Shih, Crack tip and associated domain integrals from momentum and energy balance, Engrg. Fract. Mech. 27 (1987) 615–642.
[11] B. Moran and C.F. Shih, A general treatment of crack tip contour integrals, Int. J. Fracture 35 (1987) 295–310.
[12] H. Tada, P.C. Paris and G.R. Irwin, The Stress Analysis of Cracks Handbook (Del Research Corporation, Hellertown, PA, 1973).